BENDING BEHAVIOR OF SHORT STEEL CYLINDERS UNDER AXIAL FORCE FLUCTUATIONS

Osman Tunc CETINKAYA*, Shozo NAKAMURA**, Kazuo TAKAHASHI***

*Graduate Student, Nagasaki University Graduate School of Science and Technology (1-14, Bunkyo-machi, Nagasaki 852-8521)

****Corresponding Author, Associate Professor, Nagasaki University, Department of Civil Engineering (1-14, Bunkyo-machi, Nagasaki 852-8521) E-mail: snakamura@civil.nagasaki-u.ac.jp Tel. & Fax: +81-95-819-2613**

***Professor, Nagasaki University, Department of Civil Engineering (1-14, Bunkyo-machi, Nagasaki 852-8521)

Abstract

During earthquake excitations, axial forces fluctuate together with bending moment fluctuations, especially in portal frame bridge piers and the arch-ribs of arch bridges. Conventionally, however, the axial force is treated as constant when evaluating the capacity of structures under seismic loading. In this paper, the influence of axial force fluctuations on the maximum strength and ductility of short steel cylinders is considered in an effort to establish practical formulations for the seismic design of steel bridge members with pipe sections. Elastoplastic large-displacement analysis is carried out on parametric models generated by setting the radius-thickness ratio as the main structural parameter. Bending behavior under constant and fluctuating axial force is compared, where the final value of considered axial force fluctuation is the same as the axial force magnitude in the constant axial force case. It is found that the moment and ductile capacity corresponding to the post-peak region of bending behavior are significantly improved when the axial force fluctuation is considered. Design formulae for failure strain taking into account this capacity improvement are proposed for different limit states. The validity of the proposed formulae is demonstrated through numerical analysis.

Keywords: *Short cylinders, axial force fluctuation, elastoplastic large displacement analysis, seismic design, steel bridges.*

1. Introduction

Steel pipe sections are widely employed in bridges on Japan's road network, especially in cantilever bridge piers. They are susceptible to loss of capacity with the occurrence of local buckling, since such sections are generally characterized by a large ratio of radius to component plate thickness. This kind of damage was observed extensively during the Hyogo-ken Nanbu Earthquake in the shape of so-called ‘elephant-foot’ buckling [1].

In the latest Japanese design code for highway bridges (JRA code) [2], published after the Hyogo-ken

Nanbu Earthquake, a performance-based seismic design method is specified in which the structural seismic demand is compared with the capacity of the members. The capacity of the steel components must be determined based on the results of cyclic loading tests using specimens or through analysis capable of considering local buckling effects. In practice, the results of investigations that include loading tests or numerical evaluations of similar structure are used instead of time-consuming cyclic loading tests or elastoplastic large-displacement analysis. But there is a great need for simplified calculation methods able to express the ultimate strength and deformation of structural members. In particular, ductile capacity is very important since deformation-based design is a more rational approach to seismic design for extreme ground motions.

Some previous investigations have involved the study of the ductility of cylinders subjected to pure compression or bending [3- 6]. As for steel bridge piers subjected to combined compression and bending, a number of experiments and numerical analyses have shown that local buckling of thin-walled steel structures always happens in the compressive flange within the effective failure range [7-10] and that maximum structural ductility is governed by the capacity of this critical local part. The ductility of this part was investigated by Gao et al. [11] through numerical analysis of short cylinders subjected to monotonic loading. The results were compared with earlier loading test results [12] and empirical ductility equations for stub-columns, which are expected to simulate the behavior of the local buckling part, were presented. These equations were modified by Ge et al. [13] to extend their applicability to a wider range of axial force magnitudes. Their formulation is very reliable for use under constant axial force considerations. However, in many structures the axial force fluctuates considerably along with the bending moment during an earthquake. This fluctuation is significant and may have some influence on capacity, especially in portal frame bridge piers and arch bridges. Aoki et al. [14] conducted cyclic loading tests using a varying axial load on individual column specimens from portal frames. They found that ductility was slightly improved compared to the constant axial load case under a loading condition where a small amount of variation at a moderate axial force magnitude is considered. This finding suggests that different degrees of improvement may be obtained under different loading conditions. For this reason, it is necessary to evaluate the influence of axial force fluctuation on the ductility of steel members under a variety of structural and loading conditions and establish formulae that take this influence into account. Such formulae would contribute to the rationalization of seismic design taking improved ductility into account.

The main aim of this study is to develop design formulae for predicting the failure strain of short steel

cylinders under a bending load with axial force fluctuation. First, elastoplastic large-displacement analysis of parametric short steel cylinder models is carried out. Then, bending behavior in various constant and fluctuating axial force cases is compared in order to evaluate the effect of axial force fluctuation on ductility and strength. Finally, design formulae for failure strain with different limit state definitions are proposed on the basis of these results.

2. Numerical Analysis Method

2.1 Analyzed Models

The influence of axial force fluctuation on the bending behavior of short steel cylinders is examined numerically for nine models with the structural parameters listed in Table 1.

The radius-thickness ratio parameter (R_t) is adopted as the main structural parameter. It is defined by

$$R_t = \sqrt{3(1-\nu^2)} \cdot \frac{\sigma_y}{E} \cdot \frac{D}{2t} \qquad (1)$$

where, E = Young`s modulus, $\upsilon$ = Poisson`s ratio, σ_y = yield stress, D = Diameter of the cylinder and t = thickness of cylinder wall. Cylinders with R_t values ranging from 0.05 to 0.5 are generated by changing the diameter of the cylinder only, keeping an identical thickness of 20mm.

For a thin-walled cylinder subjected to compressive loading or a bending moment, buckling occurs symmetrically with respect to the axis of the cylinder in the shape of several half sine waves [15]. In this study short cylindrical segments equal in length to the critical wavelength, i.e. the length which provides the minimum ultimate strength, are adopted. The empirical formula (2) proposed by Gao et al.[11] is employed. This agrees well with Timoshenko`s elastic shell theory for obtaining critical cylinder length.

$$\frac{L}{D} = \frac{0.585}{R_t^{0.08}} - 0.580 \qquad (2)$$

The short cylinders are modeled and analyzed using general purpose MARC [16] nonlinear FE analysis software. Because of the symmetry about the midsurface in the longitudinal direction, only half of each cylinder needs to be modeled, since the buckling localization phenomenon does not take place for cylinders where the length/radius ratio is less than 1 [17, 18]. A type of four-node doubly curved shell element (No. 75) included in the MARC element library is adopted for cylinder modeling. The finite element mesh of a cylinder model is shown in Fig. 1. The numbers of divisions in the circumferential and longitudinal directions are 90 and 10, respectively.

A type of steel stress-strain relation that includes a strain-hardening component, as proposed by Usami et al. [19], is utilized (Fig 2). Here σ_y and ε_y denote the yield stress and strain, respectively. ε_{st} is the strain at the

onset of strain hardening. E_{st} is the initial strain-hardening modulus and $E`$ is the strain-hardening modulus assumed as

$$E' = E_{st} \exp\left(-\xi \frac{\varepsilon - \varepsilon_{st}}{\varepsilon_y} \right) \quad (3)$$

where ξ = material coefficient. In this study, mild steel SS400 is utilized with σ_y = 235 MPa, E = 206 GPa, υ = 0.3, $\varepsilon_{st} = 10\varepsilon_y$ $E_{st} = E/40$ and $\xi = 0.06$.

A simply supported boundary condition is assumed for the edges of the short cylinder to ensure that local buckling takes the form of a half sine wave. The deformed configuration of an analyzed cylinder is shown in Fig. 3. It can be observed that the outward displacement takes the form of a single half wave when the symmetrical displacement in the lower part of the cylinder is taken into account.

Two kinds of initial imperfection are considered in the analyses: initial geometrical deflection due to manufacturing and residual stress due to welding. An initial imperfection in the shape of a single half wave in the outward displacement is assumed according to equation (4) since a deflection pattern having the same shape as the buckled geometry will lead to the most unfavorable bending behavior.

$$w = w_{\max} \sin\left[\frac{\pi}{L}\left(\frac{L}{2} - z\right)\right] \quad (4)$$

Here, w is the outward displacement at coordinate z starting from the bottom of the half cylinder and w_{max} is the maximum outward displacement. Both the moment capacity and ductility decreases with increasing w_{max}. Here, w_{max} is taken as $0.0025L$, a realistic value that is the average of the measured maximum deflections of test specimens in a prior experimental study [12]. Geometrical imperfections in the circumferential direction are not considered as they have been observed to have no significant influence on the maximum strength and ductility of short cylinders [11].

In this analysis, an idealized form of the residual stress distribution due to welding is employed, as illustrated in Fig. 4. The welding point is arranged to be on the compression side so as to obtain a conservative estimate of capacity.

2.2 Loading Conditions

In many structures, axial force fluctuates significantly together with the bending moment during an earthquake. A typical fluctuation pattern is given in Fig. 5, which shows the relationships between axial force and bending moment for a portal frame bridge pier and for the arch-rib of a deck-type steel arch bridge under in-plane excitations. It can be seen that both relations have a linear form, although the one for the arch bridge is more complicated because of the complexity of the structure.

In this study, the monotonic loading shown in Fig. 6 is adopted as an idealization of this kind of cyclic fluctuation. During loading, the axial force and bending moment increase together in a linear manner. They reach their maximum values at the same instant and start decreasing together after that. Although the axial force and bending moment relationship tends to be more complicated in arch bridges due to the contribution of the higher modes to the overall response, the loading condition used here is considered to be sufficient, as it will lead to conservative capacity estimations.

In order to simulate the axial force fluctuation, an eccentric displacement load (P_δ) that results in linear axial force and bending moment increments at upper segment center of the cylinder is applied, as shown in Fig. 7. The top of this upper segment is constrained as a rigid plane and linked to the center node to impose bending of the cylinder. A load (P_i) that accounts for the initial value of the axial force fluctuation is applied to this node and the final axial force (P_f) is adjusted to the desired value by adjusting the eccentricity (e). The results are compared with the constant axial force case, in which the final axial force of the fluctuating axial force case is applied to the center node as a fixed value. In the constant axial force case, bending behavior is obtained by applying rotation increments to the center node**.**

It should be noted that the moment is assumed to have a uniform distribution in both the fluctuating and constant axial force loadings, as shown in the sketch in Fig. 8a, whereas seismic action would cause a moment gradient in steel bridge piers. This assumption is based on a study by Zheng at al. [10] who pointed out that although the bending moment capacity increases with a decrease in moment gradient (defined as M_1/M_2 in Fig. 8b), the ductility changes slightly. Furthermore, the cylinders in this study are quite short compared to their diameters, making the influence of the moment gradient quite negligible.

The main focus in this paper is on evaluating the influence of the axial force fluctuation on ductility. This is represented by the failure strain, which is defined as the average strain at the outmost edge on the compressive side and is calculated by

$$\varepsilon = \frac{2u}{L} \tag{5}$$

where u = longitudinal displacement of the upper or lower end of the compressive side (point A in Fig. 8a) and L = length of the short cylinder.

2.3 Axial Force Fluctuation Parameters

Analyses with different axial force fluctuation patterns are carried out for three different final axial force levels, as illustrated in Table 2**.** The amount of axial force fluctuation (α) is the ratio of final axial force (P_f) to

initial axial force (P_i). Different α-values are obtained by changing the initial axial force for a given final axial force level. Additionally, analysis with constant axial force, which is represented by $\alpha = 1$, is carried out for each final axial force case. The final axial force values are selected as 20%, 40% and 60% of the squash load (P_y) of the cylinders and for each case different fluctuation amounts of 1.5, 2 and 3 are employed. These axial force fluctuation parameters are considered to represent a wide range of realistic values of axial force fluctuations that can take place in the sections of steel bridges under severe earthquake excitations.

3. Influence of Axial Force Fluctuations

3.1 Verification of loading conditions

The various different axial force patterns are illustrated in Fig. 9 together with the corresponding bending behavior for Model 4 ($R_t = 0.125$) with respect to the rotation of the section when the final axial force is $0.6P_y$. All axes are normalized by their values at the yield state. It can be seen that the maximums of axial force and bending moment take place at the same rotational instants and that variations in bending moment and axial force are similar to the assumed monotonic loading condition shown in Fig. 6. This suggests that simulation by eccentric loading is an efficient analogy for considering axial force fluctuations in short cylinder models.

3.2 Moment-rotation relationship

In the bending behavior of Model 4 shown in Fig. 9 it can be observed that the ultimate moment capacities of constant axial force and different fluctuating axial force cases are the same. However, there is significant difference after the maximum moment is reached. In the post-peak region, the moment for fluctuating axial force cases is observed to drop more slowly, resulting in higher ductility which is more significant for higher amounts of fluctuation. The axial force in the fluctuating axial force case decreases after the peak value, whereas it is maintained even after the maximum load in the constant axial force case. This induces the difference in moment-rotation relationships in the post-peak region. Although the constant axial force case is a more severe loading condition resulting in conservative design, it is more realistic to take the axial force fluctuation and the corresponding reduction in the post-peak region into consideration, leading to more rational design of steel sections.

3.3 Ductility

There are some design codes which allow for post-peak behavior up to 95% [20], 90% [20] and even as far as 80% [21] of the moment capacity. In order to study the ductility improvement at different post-peak locations, limit states in the present study are selected by defining the failure strain as the strain corresponding to the 95%, 90% and 80% of maximum post-peak moment, namely M_{95}, M_{90}, M_{80} (See Fig. 10). The ductility

in constant and fluctuating axial force cases at these limit states is compared for a given final axial force level in Table 2. The comparison is illustrated in Fig. 11, where the ratio of failure strain for the axial force fluctuation case under consideration to that of the corresponding constant axial force case is plotted with respect to the R_t parameter for all final axial force levels. It can be seen that the improvement obtained by considering the effect of axial force fluctuation in post-peak ductility is valid for all models. The improvement is directly proportional to the final axial force level and the amount of axial force fluctuation. These two tendencies are more obvious when further post-peak behavior is considered. It can be also seen that the results follow a similar path with respect to the R_t value, although the ratio is larger when R_t is between 0.06 and 0.1. Excluding these scattered values, the overall trend of the improvement ratio can be approximated by the curves shown in the figure.

3.4 Comparison with existing numerical results

To verify the validity of the obtained results, normalized failure strain ($\varepsilon_u/\varepsilon_y$) in the constant axial force case is compared with values computed using formula (6) given by Ge et al. [13] for 95% of the ultimate post-peak strength, treating the axial force as a constant value.

$$\frac{\varepsilon_u}{\varepsilon_y} = \frac{0.14(1.1 - P/P_y)^{1.8}}{(R_t - 0.03)^{1.4}} + \frac{3}{(1 + P/P_y)^{0.7}} \le 20 \quad (0 \le P/P_y \le 1.0,\ 0.03 \le R_t \le 0.5) \qquad (6)$$

Fig. 12 illustrates this comparison for the constant axial forces of $0.1P_y$, $0.2P_y$ and $0.3P_y$. Additionally the individual normalized failure strains obtained in the present study are compared with those given by Gao et al. [11] in Table 3. It is seen that the results show sufficiently good agreement.

4. Design Formulae

4.1 Generation of formulae

Rather than generating a completely new formula, we propose accounting for the influence of axial force fluctuation in the design procedure by modifying the existing constant axial force formula with appropriate correction functions.

The correction functions are developed based on curves approximating the relationship shown in Fig. 11. These curves are obtained by using the least squares method to approximate all analysis results for one α-value as a power function of R_t. The individual curve functions are combined into a single function for each limit state and given as equations (7-9) using the influence of the amount of axial force fluctuation and the final axial force level to position the curves.

$\boldsymbol{M_{95}}$

$$f(R_t, P_f / P_y, \alpha) = \frac{(0.095\alpha + 0.024)P_f / P_y + 1.001}{R_t[(0.017\alpha + 0.007)P_f / P_y - 0.006\alpha - 0.003]} \geq 1 \quad , \quad 0.05 \leq R_t \leq 0.5 \qquad (7)$$

$\boldsymbol{M_{90}}$

$$f(R_t, P_f / P_y, \alpha) = \frac{(0.193\alpha + 0.05)P_f / P_y + 0.981}{R_t[(0.003\alpha + 0.007)P_f / P_y - 0.005\alpha - 0.003]} \geq 1 \quad , \quad 0.05 \leq R_t \leq 0.5 \qquad (8)$$

$\boldsymbol{M_{80}}$

$$f(R_t, P_f / P_y, \alpha) = \frac{(0.396\alpha + 0.028)P_f / P_y + 0.967}{R_t[(0.004\alpha - 0.043)P_f / P_y - 0.013\alpha + 0.018]} \geq 1 \quad , \quad 0.05 \leq R_t \leq 0.5 \qquad (9)$$

By using these proposed correction functions (7-9), it is possible to estimate the failure strain in consideration of the axial force fluctuation effect for a given R_t value and given axial force fluctuation parameters if the corresponding value for the constant axial force case is known. Equation (6) may be utilized as the formula for the constant axial force case, but it is available only for the limit state corresponding to M_{95} (See Fig. 10.). For the other two limit states, similar equations are generated as shown below:

$\boldsymbol{M_{90}}$

$$\frac{\varepsilon_u}{\varepsilon_y} = \frac{0.13(1.57 - P/P_y)^{2.62}}{(R_t - 0.03)^{1.25}} + \frac{3.30}{(1 + P/P_y)^{1.48}} \leq 20 \quad (0 \leq P/P_y \leq 0.6,\ 0.05 \leq R_t \leq 0.5) \qquad (10)$$

$\boldsymbol{M_{80}}$

$$\frac{\varepsilon_u}{\varepsilon_y} = \frac{0.25(1.56 - P/P_y)^{2.89}}{(R_t - 0.03)^{1.19}} + \frac{4.54}{(1 + P/Py)^{2.29}} \leq 20 \quad (0 \leq P/P_y \leq 0.6,\ 0.05 \leq R_t \leq 0.5) \qquad (11)$$

Estimates of failure strain obtained with the newly developed constant axial force case formulae of M_{90} and M_{80} are compared with the results of analysis for various constant axial force magnitudes in Fig. 13. Results for the pure bending case ($P/P_y = 0$) are also plotted. The equations result in fairly accurate and conservative estimates for axial forces of moderate magnitude, whereas the formulae tend to give inaccurate results for axial forces more than $0.6P_y$. It should be noted that such high axial force levels are not usually considered in the design procedure. The upper limit for the estimation of normalized failure strain is set at 20, a realistic value similar to equation (6) given by Ge et al., since higher failure strains may cause problems due to low cycle fatigue or brittle fracture although there is no risk of local buckling.

4.2 Estimation of ductility using proposed formulae

The main steps involved in estimating failure strain using the proposed formulae are summarized below and illustrated in Fig. 14.

1) Calculate the seismic demand of the structure and get the initial (P_i) and maximum (P_f) values of axial force occurring in the pipe section under consideration.

2) With the assumption of monotonic loading, calculate the α-value defined as P_f / P_i using the values

obtained in 1).

3) Estimate the failure strain using the constant axial force case formula (equations (6), (10), (11)) for the desired limit states by substituting the maximum axial force P_f for P.

4) Calculate the value of the correction function (equations (7), (8), (9)) for the corresponding limit state using the axial force fluctuation parameter in 2). Then multiply the obtained value with the result of 3) to get the final estimates.

4.3 Application range of the estimation

The range of loading conditions for which estimations with the proposed formulae are applicable is investigated by evaluating the accuracy of the estimates for axial force fluctuation patterns not considered during the generation of the correction functions. A wide range of realistic cases are studied by adding different amounts of axial force fluctuation to the initial axial force levels of $0.1P_y$, $0.2P_y$, $0.3P_y$ and $0.4P_y$, as shown in Table 4. Within the range of α-values from 1.25 to 4, most of the estimates are found to be on the conservative side, with an error of less than 20% if the final axial force does not exceed $0.6P_y$ (the upper applicable limit of the constant axial force case formulae). This region is specified as the applicable range of the estimation and is marked in Table 4**.** Outside this region, the accuracy of estimates is low and there are many cases for which estimates on the safe side cannot be achieved. In Fig. 15, the accuracy of estimates within the applicable range is illustrated by plotting estimates against analysis results. It can be seen that conservative and fairly accurate estimations are achieved especially when the failure strain is between 5 and 20, which is the preferred ductility range for seismic design considerations.

Although the proposed formulae cover a wide range of R_t values from 0.05 to 0.5, the requirement for high ductility in design limits the practical application range of the proposed formulae in terms of R_t. In practice, R_t values between 0.05 and 0.11 find most common application for pipe sections in steel bridge piers. On the other hand, $R_t = 0.3$ can be set as a reliable upper limit since there has been a study [6] in which the validity of large-displacement finite element analysis for large-diameter steel cylinders with R_t as much as 0.3 is verified through comparison with test results.

Investigations have revealed that the ultimate ductile capacity decreases when the length of the strain plateau increases and when the slope of strain hardening diminishes. Since the steel (type SS400) used in this numerical analysis has a relatively long yield plateau ($\varepsilon_{st} = 10\varepsilon_y$) and a small strain hardening slope ($E/40$) compared to other types of steel used in Japan, the proposed formulae are considered applicable also for conservative estimates of different steel types.

4.4 Efficiency of the proposed formulae

The proposed formulae increase the efficiency of limit state design by magnifying the failure strain obtained with the constant axial force assumption using correction functions accounting for the influence of axial force fluctuations. This leads to design with a higher radius-thickness ratio for a given ductility demand. Table 5 contains limit values of R_t for certain required ductility values for three limit states. For a given ductility demand, the limit values of R_t can be obtained from this table. For example, if the normalized failure strain is required to be more than 8 under the conditions of P_f/P_y=0.2 and α=3 for the M_{95} limit state, the R_t value should not exceed 0.097, which is a higher value than the $\alpha = 1$ case. It is seen that the increase in the limit R_t value becomes more noticeable when the amount of axial force fluctuation is larger and when higher axial force magnitudes are considered. The table illustrates the limit values only for moderate final axial force magnitudes, i.e. less than $0.3P_y$. The efficiency improvement will be more obvious for higher axial force levels between $P_f/P_y = 0.3$ and $P_f/P_y = 0.6$.

5. Conclusions

This study involved the elastoplastic large-displacement analysis of short steel cylinders subjected to a bending moment together with axial force fluctuations. The bending behavior of the cylinders was compared with the conventional constant axial force case and the dominant factors in the observed difference were clarified. Based on he results of this examination, design formulae that take into account axial force fluctuations were developed for the estimation of steel pipe failure strain under three different limit states. The accuracy of the formulae was evaluated through additional numerical analysis. Limit R_t values for a given ductility requirement were tabulated for moderate final axial force cases. The findings can be summarized as follows.

1) Ductility and strength corresponding to post-peak behavior are improved when axial force fluctuations are considered.

2) The improvement in ductility is greater for higher axial force magnitudes and for larger axial force fluctuations.

3) The proposed formulae can be used to determine the ductility capacity of pipe section columns in portal frames and arch-ribs in arch bridges subjected to bending as well as axial force fluctuations during earthquakes.

4) The consideration of axial force fluctuations using the proposed formulae will result in the use of higher ductile capacities as design values compared with conventional practice, making the seismic design more

rational.

Together with pipe sections, hollow boxes are also very widely employed in steel bridges. Similar improvements in ductility are thought possible by considering the effects of axial force fluctuations for box sections. The scope of future investigations will be extended to stub box columns with and without stiffeners and design formulae will be generated for those sections.

Acknowledgements

This research is supported by a grant from the Student Research Promotion Project of the Japan Iron and Steel Federation, which is gratefully acknowledged. The authors would also like to thank Associate Prof. Hanbin Ge of Nagoya University for his kind help during the selection of the correct material model for this study.

References

[1] Watanabe E, Sugiura K, Nagata K, Kitane Y. Performances and damages to steel structures during the 1995 Hyogoken-Nanbu earthquake. Engineering Structures 1998;20(4-6):282-290.

[2] Japan Road Association (JRA). Specifications for highway bridges, Part V. Seismic design, Tokyo, Japan; 2002.

[3] Greiner R, Guggenberger W. Buckling behavior of axially loaded cylinders on local supports-with and without internal pressure. Thin-Walled Structures1998;31:159-167.

[4] Peek R. Axisymmetric wrinkling of cylinders with finite strain. Journal of Engineering Mechanics (ASCE) 2000;126(5):455-461.

[5] Kulak GL. Tubular members-large and small. Engineering Structures1996;18(10):745-751.

[6] Chen Q, Elwi AE, Kulak GL. Finite element analysis of longitudinally stiffened cylinders in bending. Journal of Engineering Mechanics (ASCE) 1996;122(11):1060-1068.

[7] Gao S, Usami T, Ge H. Ductility evaluation of steel bridge piers with pipe sections. Journal of Engineering Mechanics (ASCE) 1998;124(3):260-267.

[8] Nishikawa K, Murakoshi J, Takahashi M, Okomoto T, Ikeda S Morishita H. Experimental study on strength and ductility of steel portal frame pier. Journal of Structural Engineering (JSCE) 1999;45A:235-244 [in Japanese].

[9] Nishikawa K, Yamamoto S, Natori T, Terao O, Yasunami H, Terada M. An experimental study on improvement of seismic performance of existing steel bridge piers. Journal of Structural Engineering (JSCE) 1996;42A:975-986 [in Japanese].

[10] Zheng Y, Usami T, Ge H. Ductility evaluation procedure for thin-walled steel structures. Journal of Structural Engineering (ASCE) 2000;126(11): 1312-1319.

[11] Gao S, Usami T, Ge H. Ductility of steel short cylinders in compression and bending. Journal of Engineering Mechanics (ASCE) 1998;124(2):176-183.

[12] Usami T, Aoki T, Kato M, Wada M. Failure test on tubular steel stub-column in compression and in bending. Proceedings of JSCE (Structural Engineering/Earthquake Engineering) 1990; 416(I-13):255-65. [in Japanese]

[13] Ge H, Kono T, Usami T. Failure strain of steel segments subjected to combined compression and bending and application to dynamic verification of steel arch bridges. Journal of Structural Engineering (JSCE) 2004;50A:1479-1488 [in Japanese].

[14] Aoki T, Susantha KAS. Seismic performance of rectangular-shaped steel piers under cyclic loading. Journal of Structural Engineering (ASCE) 2005;131(2):240-249.

[15] Timeshenko SP, Gere JM. Theory of elastic stability. McGraw-Hill; 1961.

[16] MARC Analysis Research Corporation. MARC User Manual Volume A- Volume E, version K7.; 1997.

[17] Goto Y. Analysis of localization of plastic buckling patterns under cyclic loading. Engineering Structures 1998;20(4-6):413-424.

[18] Goto Y, Chonghou Z, Qingyun W, Makoto O. A rigorous method for the analysis of localization of axisymmetric buckling patterns in thick cylindrical shells. Thin-Walled Structures1998;31: 73-88.

[19] Usami T, Suzuki M, Mamaghani IHP, Ge H. A proposal for check of ultimate earthquake resistance of partially concrete-filled steel bridge piers. Journal of Structural Mechanics and Earthquake Engineering (JSCE) 1995;508(I-31):69-82. [in Japanese]

[20] Railway Technical Research Institute. Seismic design code for railway structures. Maruzen; 1999 [in Japanese].

[21] California Department of Transportation (Caltrans). San Francisco-Oakland Bay Bridge west spans seismic retrofit design criteria. Sacramento (CA); 1997.

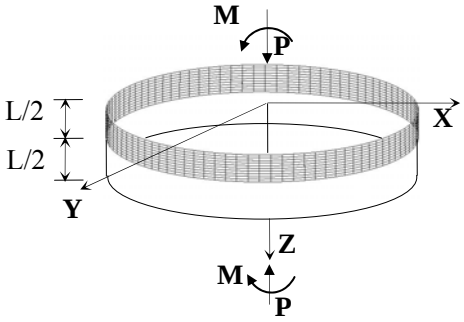

Fig. 1. Analytical model.

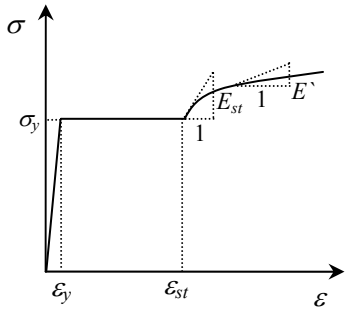

Fig. 2. Material model.

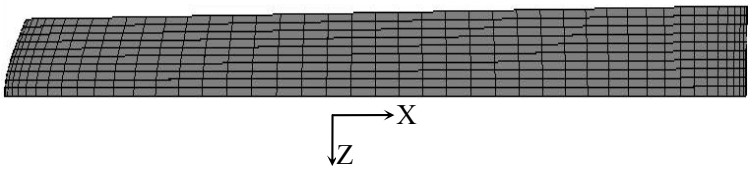

Fig. 3. Buckling mode of cylinder.

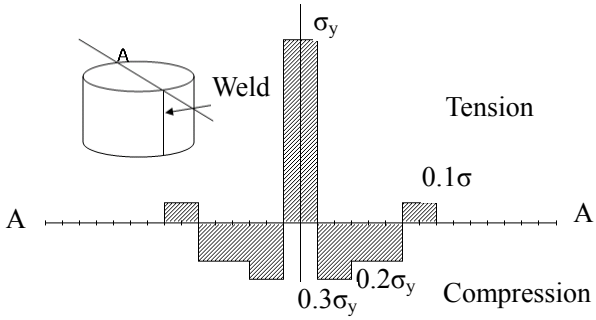

Fig. 4. Distribution of residual stress.

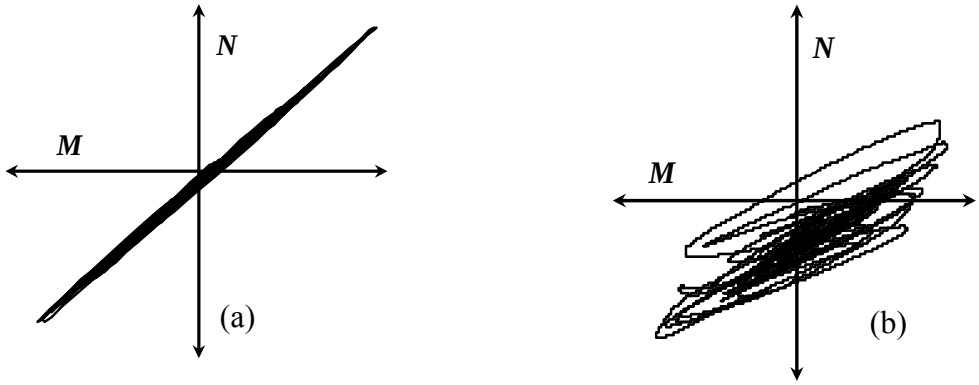

Fig. 5. Axial force-bending moment relationship (a) for a portal frame (b) for arch rib of an arch bridge.

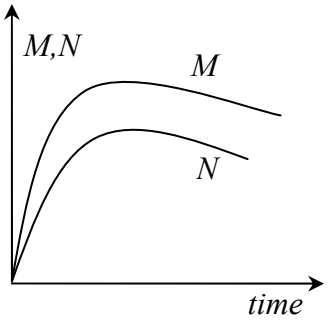

Fig. 6. Assumed monotonic loading condition.

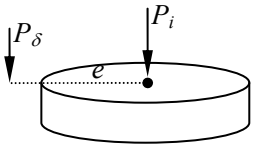

Fig. 7. Loading method for axial force fluctuation.

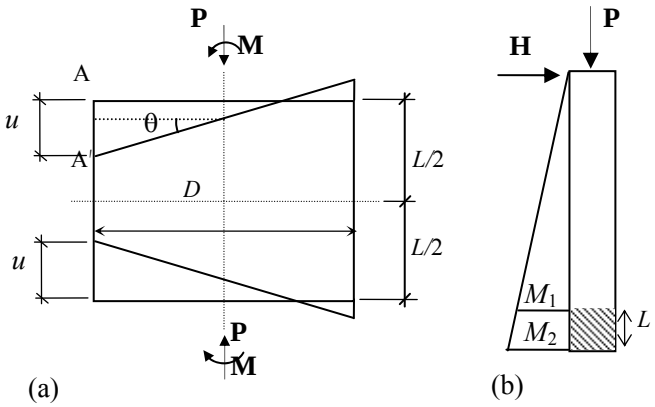

Fig. 8. Sketch of the studied short cylinder and moment gradient.

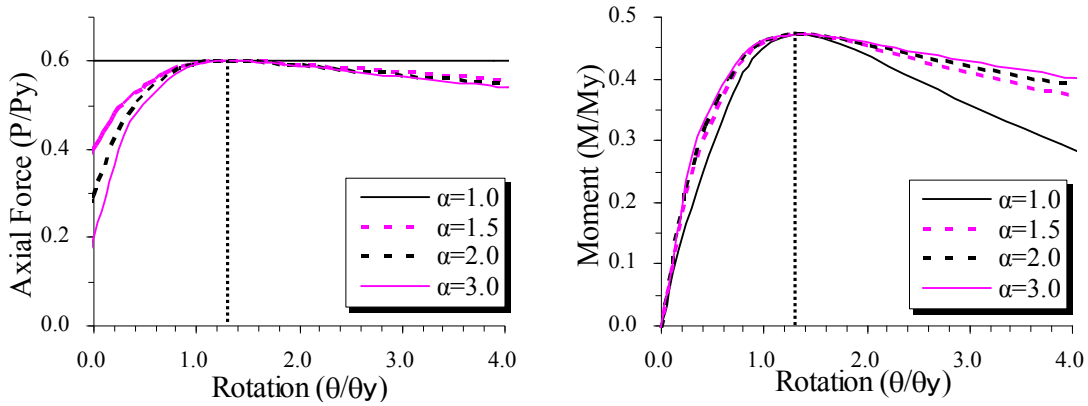

a) Axial force-rotation relationship b) Bending moment-rotation relationship

Fig. 9. Bending behavior for different α-values (Model 4).

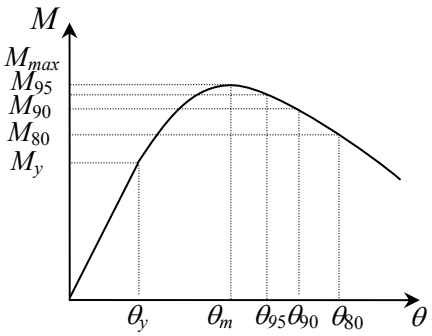

Fig. 10. Definition of limit states.

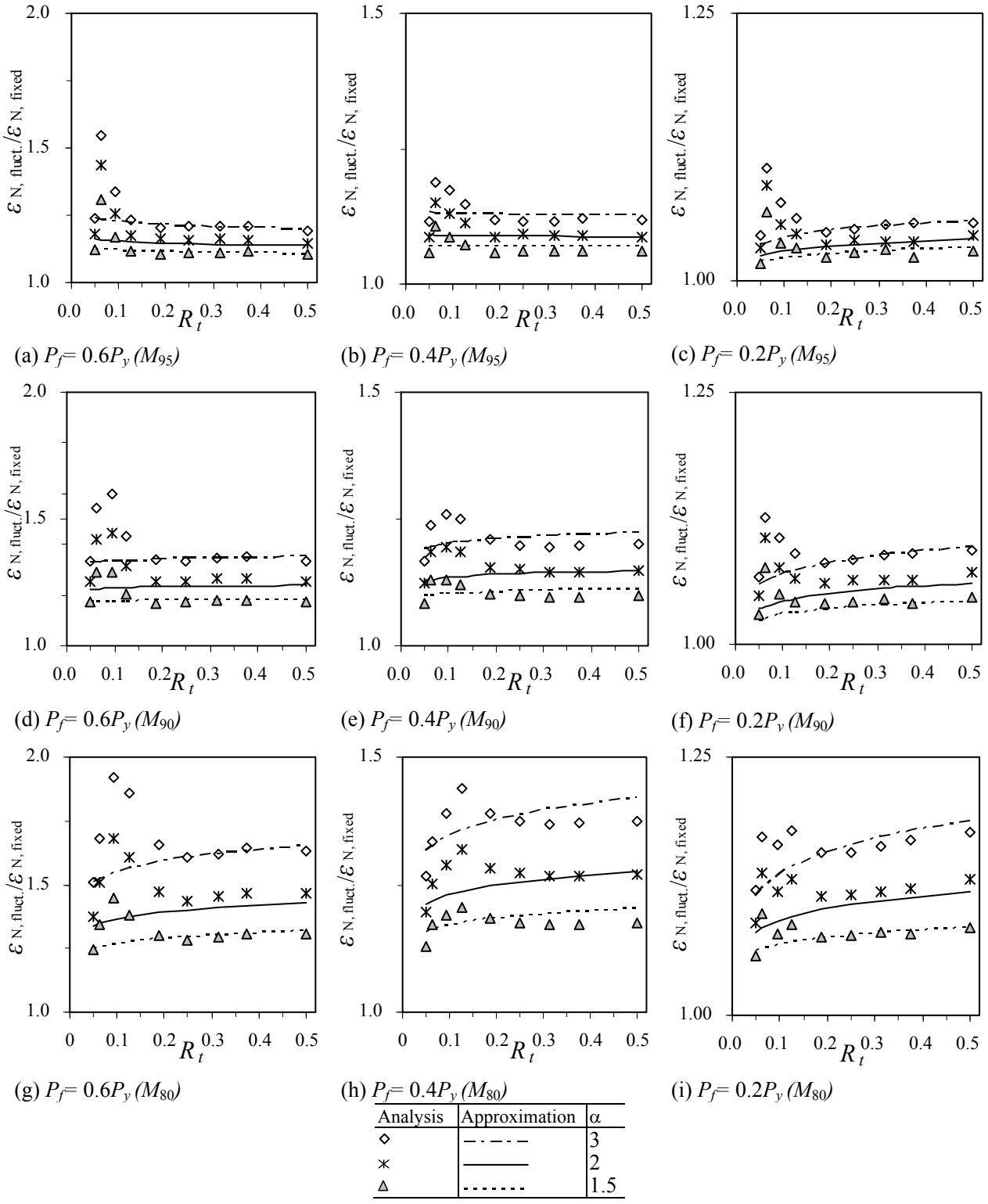

Fig. 11. Comparison of the post-peak ductility.

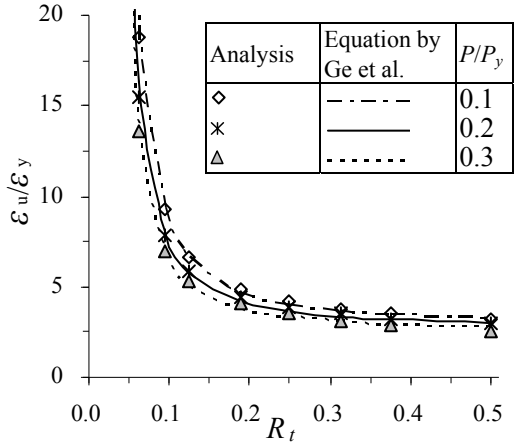

Fig. 12. Comparison with existing equation.

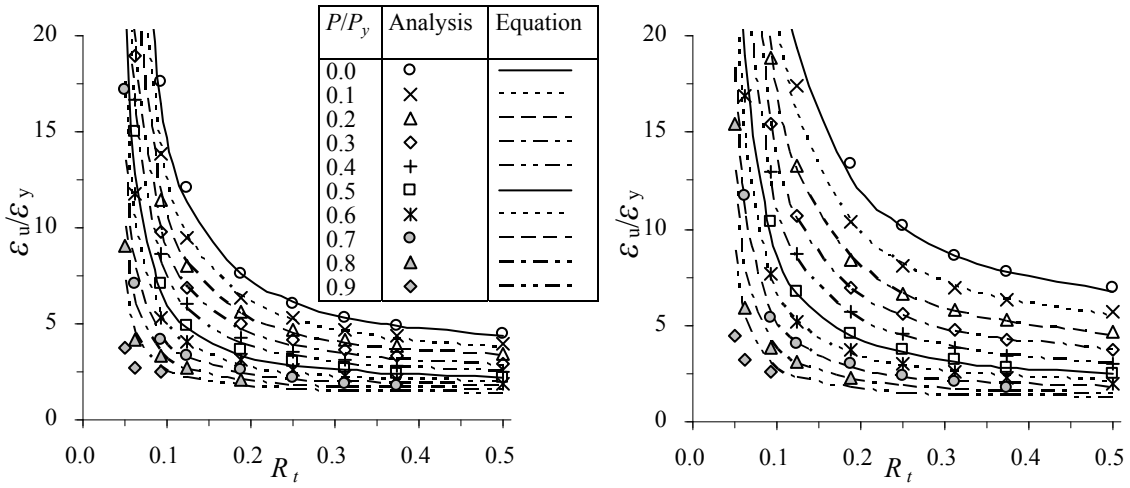

(a) M_{90} (b) M_{80}

Fig. 13. Comparison of analysis results and the proposed equation for constant axial force case.

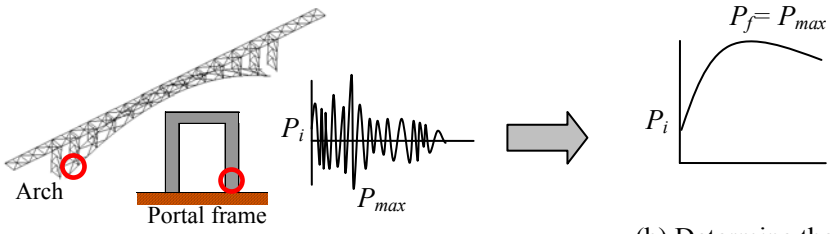

(a) Calculate the seismic demand.

(b) Determine the axial force fluctuation parameters.

$$\frac{\varepsilon_u}{\varepsilon_y} = f(R_t, \frac{P_f}{P_y}) \times f(R_t, \frac{P_f}{P_y}, \alpha)$$

(d) Use the correction functions to modify the results of the previous step to get the final estimate.

$$\frac{\varepsilon_u}{\varepsilon_y} = f(R_t, \frac{P_f}{P_y})$$

(c) Estimate the failure strain with constant axial force case formula.

Fig. 14. Outline of the estimation of ductility capacity.

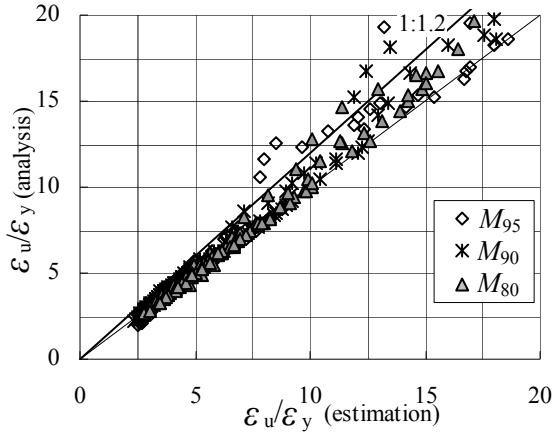

Fig. 15. Estimation accuracy.

Table 1
Structural parameters of the analyzed models

Model	Diameter (*D*-mm)	Thickness (*t*-mm)	Length (*L*-mm)	*D/t*	R_t	*L/D*
1	1062	20	173.6	53.1	0.050	0.163
2	1328	20	199.4	66.4	0.063	0.150
3	1988	20	252.5	99.4	0.094	0.127
4	2656	20	294.5	132.8	0.125	0.111
5	3980	20	353.5	199.0	0.188	0.089
6	5308	20	390.6	265.4	0.250	0.074
7	6636	20	413.1	331.8	0.313	0.062
8	7962	20	419.8	398.1	0.375	0.053
9	10616	20	407.2	530.8	0.500	0.038

Table 2
Combination of P_i and P_f

P_f	α	P_i
$0.2P_y$	1.0	$0.20P_y$
	1.5	$0.13P_y$
	2.0	$0.10P_y$
	3.0	$0.07P_y$
$0.4P_y$	1.0	$0.40P_y$
	1.5	$0.27P_y$
	2.0	$0.20P_y$
	3.0	$0.13P_y$
$0.6P_y$	1.0	$0.60P_y$
	1.5	$0.40P_y$
	2.0	$0.30P_y$
	3.0	$0.20P_y$

Table 3
Comparison with the numerical results by Gao et al.

	Results from Gao. et al.($\varepsilon_u/\varepsilon_y$)			Current study ($\varepsilon_u/\varepsilon_y$)			Gao et al./Current study		
R_t	P/P_y=0.1	P/P_y=0.2	P/P_y=0.3	P/P_y=0.1	P/P_y=0.2	P/P_y=0.3	P/P_y=0.1	P/P_y=0.2	P/P_y=0.3
0.050	–	29	22.7	31.11	25.30	22.26	–	1.1	1.0
0.063	19.3	15.2	12.3	18.80	15.43	13.60	1.0	1.0	0.9
0.094	9.05	7.4	6.68	9.24	7.85	6.97	1.0	0.9	1.0
0.125	6.54	5.75	5.24	6.59	5.82	5.33	1.0	1.0	1.0
0.188	4.78	4.43	4.08	4.83	4.46	4.12	1.0	1.0	1.0
0.250	4.14	3.83	3.52	4.15	3.86	3.54	1.0	1.0	1.0
0.313	3.78	3.54	3.09	3.77	3.49	3.14	1.0	1.0	1.0
0.375	3.61	3.36	2.87	3.52	3.25	2.88	1.0	1.0	1.0
0.500	3.52	3.17	2.71	3.22	2.94	2.58	1.1	1.1	1.1

Table 4
Applicable range of the proposed method

α	P_i=0.1P_y	P_i=0.2P_y	P_i=0.3P_y	P_i=0.4P_y
1.25	Applicable			
1.5				
2				Invalid
3			Invalid	
4		Invalid		
6	Invalid			
8	Invalid			

Table 5
Limit values of R_t for required ductility

a) M_{95}

	P_f=0.1P_y				P_f=0.2P_y				P_f=0.3P_y			
	α=1	α=1.5	α=2	α=3	α=1	α=1.5	α=2	α=3	α=1	α=1.5	α=2	α=3
$\varepsilon_u/\varepsilon_y$=5	0.170	0.171	0.171	0.171	0.146	0.150	0.152	0.154	0.126	0.132	0.134	0.138
$\varepsilon_u/\varepsilon_y$=6	0.137	0.137	0.137	0.137	0.120	0.123	0.124	0.125	0.105	0.110	0.111	0.113
$\varepsilon_u/\varepsilon_y$=8	0.106	0.106	0.106	0.106	0.095	0.096	0.097	0.097	0.085	0.087	0.088	0.089
$\varepsilon_u/\varepsilon_y$=10	0.090	0.090	0.090	0.090	0.082	0.083	0.083	0.083	0.074	0.076	0.076	0.077
$\varepsilon_u/\varepsilon_y$=20	0.062	0.062	0.062	0.062	0.058	0.058	0.058	0.059	0.054	0.055	0.055	0.055

b) M_{90}

	P_f=0.1P_y				P_f=0.2P_y				P_f=0.3P_y			
	α=1	α=1.5	α=2	α=3	α=1	α=1.5	α=2	α=3	α=1	α=1.5	α=2	α=3
$\varepsilon_u/\varepsilon_y$=5	0.269	0.270	0.273	0.279	0.213	0.224	0.229	0.239	0.173	0.188	0.194	0.206
$\varepsilon_u/\varepsilon_y$=6	0.206	0.206	0.207	0.211	0.169	0.176	0.179	0.185	0.142	0.152	0.156	0.163
$\varepsilon_u/\varepsilon_y$=8	0.148	0.148	0.149	0.150	0.127	0.131	0.132	0.136	0.109	0.115	0.118	0.122
$\varepsilon_u/\varepsilon_y$=10	0.121	0.121	0.121	0.122	0.106	0.108	0.109	0.111	0.093	0.097	0.098	0.102
$\varepsilon_u/\varepsilon_y$=20	0.075	0.075	0.075	0.075	0.068	0.069	0.070	0.071	0.062	0.064	0.065	0.066

c) M_{80}

	P_f=0.1P_y				P_f=0.2P_y				P_f=0.3P_y			
	α=1	α=1.5	α=2	α=3	α=1	α=1.5	α=2	α=3	α=1	α=1.5	α=2	α=3
$\varepsilon_u/\varepsilon_y$=5	–	–	–	–	0.396	0.468	0.505	0.595	0.282	0.348	0.379	0.453
$\varepsilon_u/\varepsilon_y$=6	0.411	0.432	0.445	0.474	0.291	0.329	0.345	0.383	0.220	0.260	0.277	0.314
$\varepsilon_u/\varepsilon_y$=8	0.257	0.265	0.269	0.278	0.200	0.218	0.225	0.241	0.160	0.182	0.190	0.208
$\varepsilon_u/\varepsilon_y$=10	0.195	0.200	0.202	0.206	0.158	0.170	0.174	0.183	0.130	0.145	0.150	0.162
$\varepsilon_u/\varepsilon_y$=20	0.105	0.106	0.106	0.107	0.091	0.095	0.096	0.099	0.079	0.085	0.087	0.091